

# THE $\tau$ ONE-PRONG PROBLEM AND RECENT MEASUREMENTS BY THE HRS COLLABORATION

J. Repond  
Argonne National Laboratory  
Argonne, IL 60439

## Abstract

We summarize recent measurements by the HRS collaboration of the topological branching fractions, the production cross section, the lifetime, and the rate into electrons of the  $\tau$  lepton. An inconsistency with theoretical expectations persists at the level of two standard deviations.

## Introduction

The study of the production and decay properties of the  $\tau$  lepton is of particular interest in view of the long-standing discrepancy between the inclusive decay branching fraction into one charged particle and the sum of the exclusive one-prong final state. The problem was first noticed by T. Truong<sup>1)</sup> in 1984 and, despite recent precise measurements of the quantities involved, no convincing solution has emerged.

We briefly outline the measurements of the topological branching fractions, production cross section, lifetime and rate into electrons of the  $\tau$  lepton by the High Resolution Spectrometer (HRS) collaboration. The results are based on data corresponding to an integrated luminosity of about  $300\text{pb}^{-1}$  which were collected at a center-of-mass energy  $\sqrt{s} = 29\text{ GeV}$  at the PEP  $e^+e^-$  storage ring. We summarize the results by comparing the values to theoretical expectations.

## Production Cross Section and Topological Branching Fractions of the $\tau$ Lepton

Our group has previously published measurements of the production cross section<sup>2]</sup> and the topological branching fractions<sup>3]</sup> using data samples corresponding to integrated luminosities of  $106pb^{-1}$  and  $176pb^{-1}$ , respectively. The present analysis<sup>4]</sup> is based on the full data sample and, therefore, supercedes the old results.

The cuts applied to select  $\tau$  pair events in the 1-1, 1-3, 3-3, and 1-5 charged track topologies and to reject other annihilation channels have been described in Refs. 2 and 3. The number of events that passed these selection criteria are summarized in Table I. Also shown is the background from non- $\tau$ -pair events in the different topologies.

The detection efficiencies for the four different topological final states have been calculated by use of a Monte Carlo (MC) simulation of  $\tau$  production and decay, including the  $\alpha^3$  QED radiative corrections.<sup>5]</sup> The generated events were subject to the same cuts as applied to the data, and the resulting detection efficiencies are displayed in the last column of Table I. The errors correspond to the statistical uncertainty of the MC-generated events.

We applied two methods, a maximum likelihood fit and a  $\chi^2$  minimization, to extract the production cross section and the topological branching fractions from the numbers given in Table I. In order to simplify the calculations,  $B_5$  was fixed at the value obtained in an earlier analysis of HRS data,  $B_5 = 0.0012$ .<sup>6]</sup> With the constraint  $B_1 + B_3 + B_5 = 1$ , this reduces the unknown variables to either  $B_1$  or  $B_3$  and  $N_\tau$ , the efficiency corrected number of produced  $\tau$  pairs.

The results obtained with the two methods were identical:  $B_1 = 0.864 \pm 0.003 \pm 0.003$ ,  $B_3 = 0.135 \pm 0.003 \pm 0.003$  and  $N_\tau = 40512 \pm 543 \pm 712$ , where the first error is statistical and the second systematic. The systematic errors are dominated by the uncertainty in the efficiency calculations related to the exact values of the exclusive  $\tau$  decay branching ratios.

**Table I**  
Data and Background Summary

Topology	Number of Events	Background	Corrected Number of Events	Detection Efficiency
1-1	3643	$(7.8 \pm 0.3)\%$	3359	$(11.07 \pm 0.12)\%$
1-3	2963	$(5.8 \pm 1.1)\%$	2537	$(26.42 \pm 0.29)\%$
3-3	158	$(7.4 \pm 2.4)\%$	146	$(21.85 \pm 0.91)\%$
1-5	13	$(1.4 \pm 0.6)\%$	13	$(15.98 \pm 0.82)\%$

The production cross section ratio to the QED prediction up to the order  $\alpha^3$  is given by

$$R_{\tau\tau} = N_{\tau}/N_{\tau_{\text{calc}}} = 1.044 \pm 0.014 \pm 0.030,$$

where  $N_{\tau_{\text{calc}}} = \sigma_{\tau\tau_{\text{rad}}} \cdot \int Ldt = 38800$  is the calculated total number of  $\tau$  pairs produced. The integrated luminosity  $\int Ldt = (291 \pm 7)pb^{-1}$  was obtained from an analysis of wide angle Bhabha events.

### Measurement of the $\tau$ Lepton Lifetime

The measurement of the  $\tau$  lifetime was published in 1987 and details can be found in Ref. 7. The flight distances of 1311  $\tau$  decays to three charged particles were measured using a four-layer tubular cell vertex chamber in conjunction with the main drift chamber. The resulting  $\tau$  lifetime is  $\tau_{\tau} = (2.99 \pm 0.15 \pm 0.10) \times 10^{-13}$  sec.

Assuming lepton universality, the  $\tau$  lifetime is related to the leptonic decay branching ratio through the equation:

$$B_e = \frac{\tau_{\tau}}{\tau_{\mu}} \left( \frac{m_{\tau}}{m_{\mu}} \right)^5 \quad (1)$$

where  $\tau_{\mu,\tau}$  and  $m_{\mu,\tau}$  are the lifetimes and masses of the  $\mu$  and  $\tau$  leptons.

Applying Eq. (1) to our lifetime measurements predicts

$$B_e^{\tau} = (18.7 \pm 0.9 \pm 0.6)\%.$$

### Measurement of the Branching Ratio for $\tau^{-} \rightarrow e^{-}\bar{\nu}_e\nu_{\tau}$

The analysis<sup>8]</sup> is based on identification of electrons through the measurement of their associated electromagnetic showers in the barrel shower counter and by comparing the deposited energy to the measured track momentum.

Two different approaches were followed to extract the number of electrons in the data sample:

#### a. E/p Ratio:

Figure 1 shows the E/p ratio for all one-prong  $\tau$  decay candidates, in both the 1-1 and 1-3 charged track topologies. Here E is the total energy deposited in the module hit by the track, plus the two neighboring modules, and p is the track momentum. A clear peak is evident at E/p = 1 over a slowly falling background.

The shape of the electron peak was determined by studying radiative Bhabha events  $e^+e^- \rightarrow e^+e^-(\gamma)$  and two-photon events  $e^+e^- \rightarrow e^+e^-e^+e^-(\gamma)$  (RBE), which were

selected using a modification of the program written for the selection of the 1-1  $\tau$  pair candidates.

The form of the background was determined using an iterative method based on event mixing, as described in Ref. 8. The results of the procedure are superimposed on the data of Fig. 1: the signal as the solid line and the background as the histogram.

As an important check, this analysis technique was applied to  $\tau$ -pair events generated by our MC experiment simulation. The number of electrons and the shape of the background were both accurately reproduced.

#### b. Chi-Squared Technique:

We define a chi-squared for a track to be an electron in the following way:

$$\chi_e^2 = \left( \frac{E_3 - \bar{E}_3(p)}{\sigma_{E_3}} \right)^2 + \left( \frac{E_8 - \bar{E}_8(p)}{\sigma_{E_8}} \right)^2, \quad (2)$$

where  $E_3(E_8)$  is the energy measured by the front  $3X_o$  (rear  $8X_o$ ) section of the calorimeter. The average energy deposited in the front and rear section as a function of track momentum was measured by the RBE and parameterized as follows:

$$\bar{E}_3(p) = (0.17 + 0.43 \cdot e^{-0.36p})p, \quad (3)$$

$$\bar{E}_8(p) = p - \bar{E}_3(p).$$

The energy resolution, as a function of deposited energy for the two sections separately, was determined from the RBE events and is well described by  $\sigma_{E_3} = 37.5\sqrt{E_3}\%$  and  $\sigma_{E_8} = 46.1\sqrt{E_8}\%$ .

Using these parameterizations, the expected  $\chi_e^2$  distributions for the 1-1 and 1-3  $\tau$  decay topologies were separately determined.

Figure 2 shows the  $\chi_e^2$  distributions for the  $\tau$  data. The backgrounds under the electron signals at low  $\chi_e^2$  are mostly due to the overlap of charged pions with photons from decays such as  $\tau^- \rightarrow \rho^- \nu_\tau \rightarrow \pi^- \pi^0 \nu_\tau$ .

The shape of the background was determined using event mixing in an analogous way to the E/p-method. The resulting signals are shown as the solid lines and the backgrounds as the histograms in Fig. 2. The number of electrons obtained by the two analyses are in excellent agreement, as shown in Table II.

The background in the 1-1 sample from both two-photon events  $e^+e^- \rightarrow e^+e^-e^+e^-(\gamma)$  and from radiative Bhabha events was determined by studying the transverse momentum  $p_T$  distribution of events in which both tracks were consistent with being electrons. The distribution shows an enhancement at low  $p_T$  values in contrast to the prediction of the  $\tau$  MC. The enhancement at low  $p_T$  corresponds to  $77 \pm 10$  events or  $154 \pm 20$  electrons. The background in the 1-3 sample was determined by searching for events containing a  $e^+e^-$  pair, in addition to a converted photon. Only one background candidate was found.

The branching ratio  $B_e$  was then calculated as

$$B_e = \frac{N_e}{\epsilon_e} \cdot N_\tau,$$

where the number of  $\tau$ 's produced,  $N_\tau = 2 \cdot \sigma_{\tau\tau_{rad}} \cdot \int L dt = 79,477$ , and  $N_e$  is the background corrected number of electrons in the data sample. The integral luminosity of  $(298 \pm 5)pb^{-1}$ , corresponding to the five years of data taking, was measured both from counting the number of wide angle Bhabha events and from the number of  $\tau$  pair events assuming  $R_{\tau\tau} = 1$ .

The efficiency  $\epsilon_e$  for detecting the  $\tau \rightarrow e\nu\nu$  decay was obtained from a MC simulation of  $\tau$  production and decay, which includes  $\alpha^3$  QED radiative corrections<sup>5]</sup> and full detector simulation. Identical  $\tau$  selection criteria were applied to the fake events. The final result is  $B_e = (17.0 \pm 0.5 \pm 0.6)\%$ , where the first error is statistical and the second systematic.

**Table II**  
Summary of Results

Topology	Number of Electrons			Detection Efficiencies	$B(\tau \rightarrow e\nu\nu)$
	E/p Method	$\chi_e^2$ Method	Background		
1-1	$1296 \pm 42$	$1288 \pm 43$	$154 \pm 20$	8.49%	$(16.9 \pm 0.6)\%$
1-3	$424 \pm 25$	$423 \pm 27$	$1 \pm 1$	3.10%	$(17.2 \pm 1.0)\%$
Total	$1720 \pm 49$	$1711 \pm 51$	$155 \pm 20$	11.59%	$(17.0 \pm 0.5)\%$

### Comparison to Theoretical Expectations

Using non- $\tau$  data, most of the exclusive decay branching ratios of the  $\tau$  lepton can be related to the rate for  $\tau \rightarrow e\nu\nu$ . Table III shows the theoretical expectations as compiled in Ref. 9 for the ratios  $R_i = B_i/B_e$ , where  $B_i$  is any exclusive  $\tau$  decay branching ratio.

**Table III**

Theoretical Predictions for the Ratio of Exclusive  $\tau$  Decay Modes to  $B(\tau \rightarrow e\nu\nu)$

Decay	1-Prong Topology	3-Prong Topology	Input
$e^-\nu\nu$	1.00	0.0	—
$\mu^-\nu\nu$	0.973	0.0	Phase Space
$\pi^-\nu$	0.607	0.0	$\tau_\pi$
$K^-\nu$	0.0395	0.0	$\tau_K$
$(\pi\pi)^-\nu$	$1.26 \pm 0.12$	0.0	CVC, $\sigma(e^+e^- \rightarrow \pi^+\pi^-)$
$(K\pi)^-\nu$	$7/9(0.057 \pm 0.009)$	$2/9(0.057 \pm 0.009)$	CVC, $\sigma(e^+e^- \rightarrow \pi^+\pi^-)$ , Cabibbo Angle
$(\pi\pi\pi)^-\nu$	$1/2 \cdot R_{(\pi\pi\pi)^-}$	$1/2 \cdot R_{(\pi\pi\pi)^-}$	No Prediction
$(4\pi)^-\nu$	$0.056 \pm 0.006$	$0.251 \pm 0.060$	CVC, $\sigma(e^+e^- \rightarrow 4\pi)$
Rest	$0.02 \pm 0.02$	$(0.03 \pm 0.02) + R_{2\pi^-\pi^+2\pi^0}$	Exp. and Theory
Total	$(4.00 \pm 0.12)$ $+0.5 \cdot R_{(\pi\pi\pi)^-}$	$(0.29 \pm 0.06)$ $+0.5R_{(\pi\pi\pi)^-} + R_{2\pi^-\pi^+2\pi^0}$	

Four comments are in order here:

- The uncertainty on the sum of decay modes leading to a one-charged prong topology is dominated by the uncertainty in  $R_\rho$ , which is related to the absolute normalization of the measurement of the cross section for  $e^+e^- \rightarrow \pi^+\pi^-$  below the  $\tau$  mass.
- No reliable theoretical prediction for  $B_{(\pi\pi\pi)^-}$  is available. Following the experimental evidence that this final state proceeds dominantly via the  $a_1(1260)$  resonance, we have set the contributions to the 1- and 3-prong final states equal.
- There is no prediction or useful upper limit for the rate of  $\tau^- \rightarrow 2\pi^-\pi^+2\pi^0$ .
- The rest includes rare decays such as  $\tau^- \rightarrow (5\pi)^-\nu$ ,  $(K\pi\pi)^-\nu$ ,  $(\eta\pi\pi)^-\nu$ , etc. Note that their contribution to the sum is small compared to the overall error.

Using the total rates for the 1- and 3-prong topology of Table III, we can set up the following sets of equations:

$$B_1 = \{(4.00 \pm 0.12) + 0.5R_{(\pi\pi\pi)^-}\} \cdot B_e,$$

$$B_3 = \{(0.29 \pm 0.06) + 0.5R_{(\pi\pi\pi)^-} + R_{2\pi^-\pi^+2\pi^0}\} \cdot B_e.$$

Neglecting  $R_{2\pi^-\pi^+2\pi^0}$ , our measured values for the topological branching fractions yield:

$$B_e^t = (19.6 \pm 0.8)\%,$$

and

$$B_{(\pi\pi\pi)^-} = (15.6 \pm 2.7)\%,$$

where the errors are dominated by the error on  $R_\rho$ . Note that if either there is a substantial fraction of the decays  $\tau^- \rightarrow (\pi\pi\pi)^-\nu$  which do not proceed via the  $a_1(1260)$  resonance and/or  $R_{2\pi-\pi+2\pi^0}$  is significantly different from zero, the value for  $B_e^t$  would increase, while the value for  $B_{(\pi\pi\pi)^-}$  would decrease.

Table IV compares our different determinations of  $B_e$ . The agreement between the direct measurement  $B_e$  and the measurement via the topological branching fractions  $B_e^t$  is rather poor. The discrepancy corresponds to 2.6 standard deviations. Averaging all three methods yields  $B_e = (18.8 \pm 0.5)\%$ .

**Table IV**  
Comparison of Different Measurements of  $B_e$

Method	$B_e$	Difference with $B_e^t$	Significance
Direct measurement ( $B_e$ )	$(17.0 \pm 0.8)\%$	$(2.6 \pm 1.1)\%$	$2.3\sigma$
Lifetime measurement ( $B_e^\tau$ )	$(18.7 \pm 1.1)\%$	$(0.9 \pm 1.3)\%$	$0.7\sigma$
Average ( $B_e, B_e^\tau$ )	$(17.7 \pm 0.7)\%$	$(1.9 \pm 1.1)\%$	$1.8\sigma$
Topological Br. Fr. ( $B_e^t$ )	$(19.6 \pm 0.8)\%$	—	—
Average ( $B_e, B_e^\tau, B_e^t$ )	$(18.5 \pm 0.5)\%$	—	—

## Conclusions

We report recent measurements by the HRS collaboration of the topological branching fractions, the production cross section, the lifetime, and the decay rate into electrons of the  $\tau$  lepton. We compare the results with theoretical expectations and observe an inconsistency at the level of two standard deviations. Other groups<sup>10]</sup> have observed similar inconsistencies, but caution has to be applied when combining results from different experiments. Specifically, a recent statistical analysis<sup>11]</sup> of the global measurements of the exclusive  $\tau$  decay channels show evidence for bias. Therefore, conclusions about the confidence level of discrepancies that rest on the use of world average measurements are suspect. We conclude that the inconsistency in  $\tau$  decay is not significant enough to cast serious doubt on the Standard Model of electroweak interactions. However, a dedicated high statistics experiment with emphasis on the measurement of  $\tau$  decay modes involving neutral particles is strongly needed. A high luminosity  $\tau$ -charm factory would be an ideal tool for such a precision experiment.

This work was supported by the U.S. Department of Energy, Division of High Energy Physics, Contract W-31-109-ENG-38.

## References

1. T. N. Truong, Phys. Rev. **D30**, 1509 (1984).
2. K. K. Gan et al., Phys. Lett. **153B**, 116 (1985).
3. C. Akerlof et al., Phys. Rev. Lett. **55**, 570 (1985).
4. S. Abachi et al., ANL-HEP-PR-88-90, Phys. Rev. D. (to be published).
5. F. A. Berends and R. Kleiss, Nucl. Phys. **B177**, 237 (1981); F. A. Berends, R. Kleiss, and S. Jadach, Nucl. Phys. **B202**, 63 (1982).
6. B. G. Bylsma et al., Phys. Rev. **35**, 2269 (1987).
7. S. Abachi et al., Phys. Rev. Lett. **59**, 2519 (1987).
8. S. Abachi et al., ANL-HEP-PR-88-89, Phys. Lett. (to be published).
9. F. J. Gilman and S. H. Rhie, Phys. Rev. **D31**, 1066 (1985); F. J. Gilman, Phys. Rev. **D35**, 3541 (1987); W. J. Marciano and A. Sirlin, Phys. Rev. Lett. **61**, 1815 (1988).
10. B. C. Barish and R. Stroynowski, Phys. Rep. **157**, 1 (1988); K. K. Gan and M. L. Perl, Int. Journal of Mod. Phys. **A3**, 531 (1988).
11. K. G. Hayes and M. L. Perl, Phys. Rev. **D38**, 335 (1988).



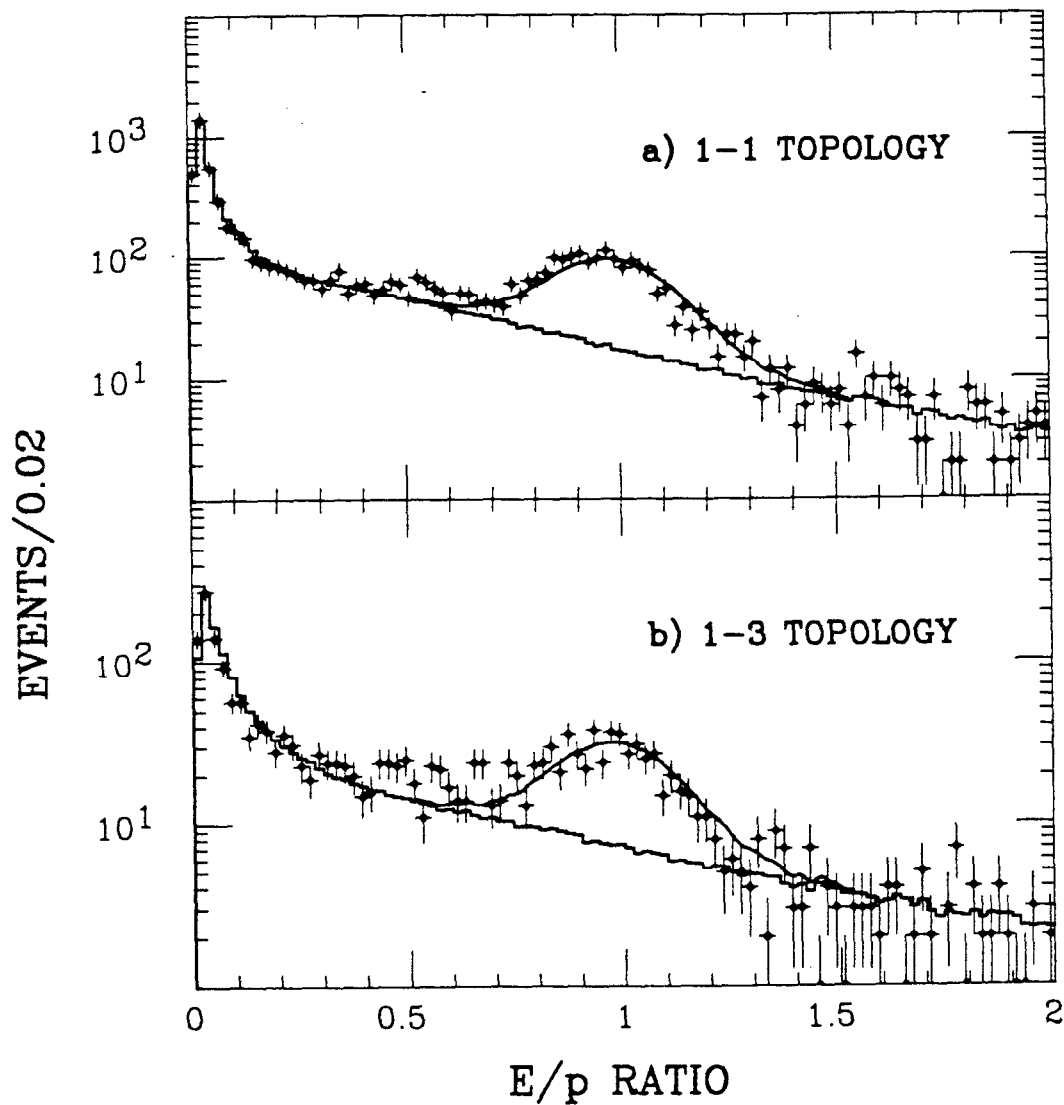


Fig. 1. Energy/momentum ratio for one-prong tau decays compared to the fits described in the text: (a) one-prong tau decays from the 1-1 decay topology, (b) one-prong tau decays from the 1-3 decay topology.

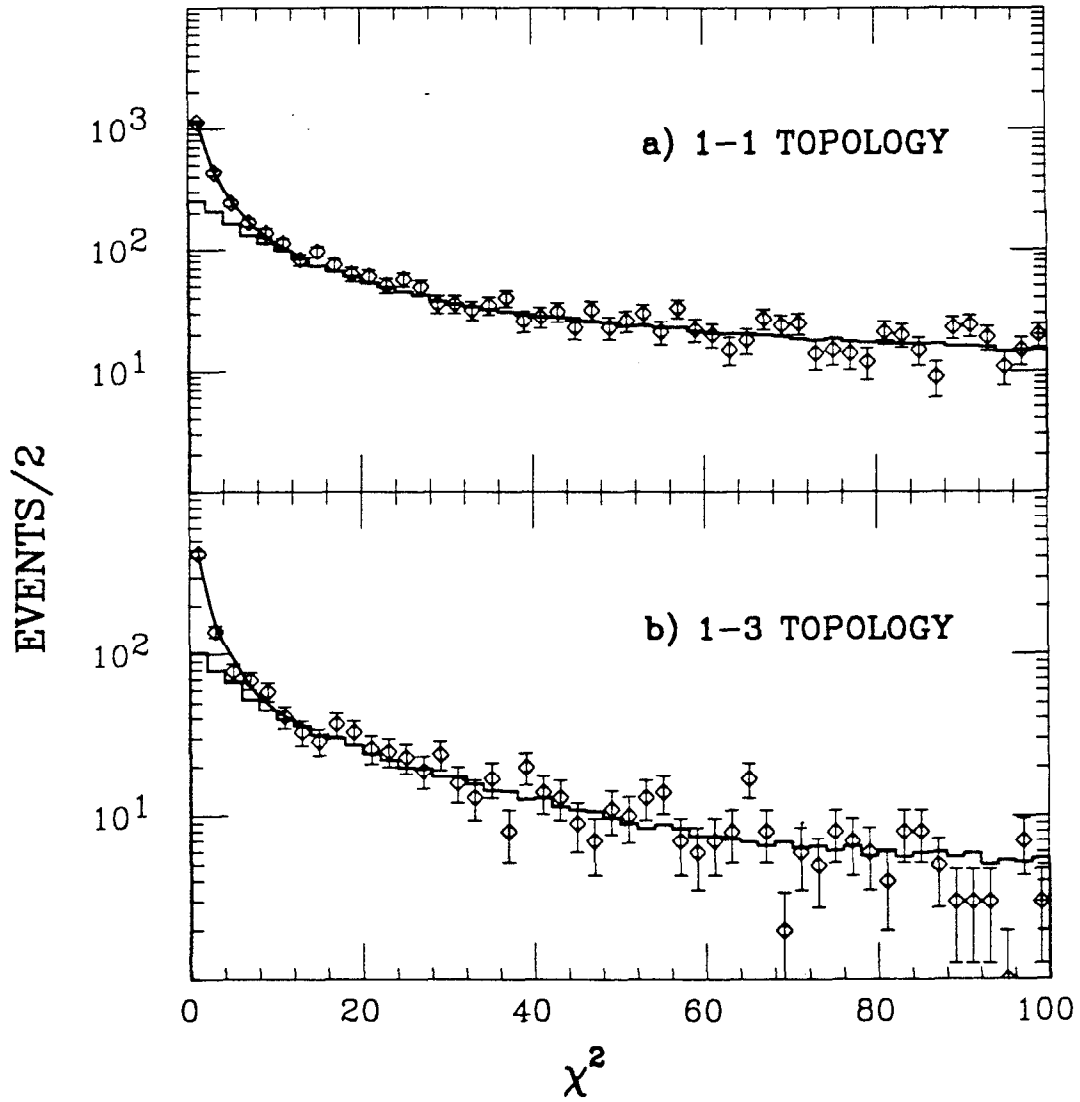


Fig. 2. Distribution in  $\chi_e^2$  (equation (2)) compared to the fits described in the text: (a) one-prong tau decays from the 1-1 decay topology, (b) one-prong tau decays from 1-3 decay topology.